Supplementary Information for:

Porous supramolecular gels produced by reversible self-gelation of ruthenium-based metal-organic polyhedra

Javier Troyano,*[a,b,c] Fuerkaiti Tayier,[a,d] Phitchayapha Phattharaphuti,[a,d] Takuma Aoyama,[e] Kenji Urayama,[e] and Shuhei Furukawa,*[a,d]

[a] *Institute for Integrated Cell-Material Sciences (WPI-iCeMS), Kyoto University, iCeMS Research Building, Yoshida, Sakyo-ku, Kyoto 606-8501, Japan*

[b] *Departamento de Química Inorgánica, Universidad Autónoma de Madrid, 28049 Madrid, Spain*

[c] *Institute for Advanced Research in Chemical Sciences (IAdChem), Autonomous University of Madrid, 28049 Madrid, Spain*

[d] *Department of Synthetic Chemistry and Biological Chemistry, Graduate School of Engineering, Kyoto University, Katsura, Nishikyo-ku, Kyoto 615-8510, Japan*

[e] *Department of Macromolecular Science and Engineering, Kyoto Institute of Technology, Matsugasaki, Sakyo-ku, Kyoto 606-8585, Japan*

Materials and methods

All chemical reagents and solvents were used without further purification.

Physical characterization

Fourier-transform infrared (FT-IR) spectroscopy data were recorded neat using a Jasco FT/IR-6100. UV-vis was measured in a V-670 spectrophotometer (JASCO). Powder X-ray diffraction data was collected using a Rigaku SmartLab diffractometer with Cu Kα radiation (λ = 1.54056 Å) in Bragg-Brentano geometry. Rheological measurements of the gels were performed using a stress-controlled AR-G2 (TA instruments, New Castle, DE, USA) rheometer by compression mode. Shearing mode was also used in a Modular Compact Rheometer MCR 502 (Anton Paar, Graz, Austria). Dynamic Light Scattering (DLS) and zeta potential measurements were performed using a Zetasizer Nano ZS (Malvern Instruments).

Aerogel formation. Super-critical CO_2 drying process was carried out on SCLEAD2BD autoclave (KISCO) using super-critical CO_2 at 14 MPa and 40 ºC.

Crystallography. Single crystal X-ray diffraction data was obtained on a Rigaku model XtaLAB P200 diffractometer equipped with a Dectris model PILATUS 200K detector and confocal monochromated Mo Kα radiation (λ = 0.71075 Å). The structure solution and refinement were performed using ShelXT[1] using Least Squares minimization operated through the Olex2[2] interface (Table S1). The coordinated DMA molecules were refined isotropically, and their hydrogen atoms were omitted. The disordered solvent molecules were accounted for using SQUEEZE. The .cif file for the structures has been submitted to the Cambridge Structural Database: CCDC 2263447. These S7 data can be obtained free of charge from The Cambridge Crystallographic Data Centre via www.ccdc.cam.ac.uk/data_request/cif

Porosity. N_2 (77 K) gas sorption isotherms were recorded on a BELSORP-max volumetric adsorption instrument from BEL Japan Inc. Prior to gas sorption measurement, the samples were activated at 120 °C for 12 h. BET surface identification (BETSI) was used for surface area calculations.[3] Pore size distributions (PSD) were estimated by NLDFT using the slit-pore shape model.

Experimental details

Synthesis of $[Ru_2(OAc)_4(THF)_2]BF_4$:

The starting cationic diruthenium complex, $[Ru_2(OAc)_4(THF)_2]BF_4$ was prepared by following a previously reported method.[4]

Synthesis of OH-RuMOP$(OH)_{12}$ crystals and bulk OH-RuMOP$[BF_4]_{12}$:

$[Ru_2(OAc)_4(THF)_2]BF_4$ (0.180 g, 0.27 mmol), 5-hydroxyisophthalic acid (0.182 g, 1.0 mmol) and Na_2CO_3 (0.020 g, 0.18 mmol), were suspended in 2 mL of a DMA, sealed in a vial, and heated at 120 °C. After 16 hours heating, brown single crystals of OH-RuMOP$(OH)_{12}$ suitable for single crystal X-ray diffraction analysis were obtained. The mixture was centrifuged, and the resulting solid was washed with DMA (3 × 10 mL), water (2 × 10 mL) and methanol (2 × 5 mL). Then, the crystals were dissolved in 4 mL of methanol with 100 µL of aqueous HBF_4 (50 wt. %). After centrifugation, the supernatant was poured into 40 mL diethyl ether, resulting in the precipitation of orange **OH-RuMOP$[BF_4]_{12}$** solid. After centrifugation, the precipitate was washed with diethyl ether (2 × 10 mL) and dried at air overnight (0.142 g, 81% yield).

General procedure to produce OH-RuMOP-based gels:

Initial **OH-RuMOP$[BF_4]_{12}$** solutions in H_2O:DMF mixtures were prepared by first dissolving **OH-RuMOP$[BF_4]_{12}$** powder in DMF and then adding water. After centrifugation to remove air bubbles, the resulting clear brown solutions were placed into a preheated oven at 80°C towards gelation.

One-pot synthesis of OH-RuMOP-gel_{OP}:

$[Ru_2(OAc)_4(THF)_2]BF_4$ (0.032 g, 0.048 mmol) was added to a previously heated (80 °C) solution of 5-hydroxyisophthalic acid (0.035 g, 0.192 mmol) in 1 mL of a H_2O:DMF (9:1, v/v) solvent mixture. After stirring, the mixture was heated at 80 °C for 24 h, resulting in the formation of a dark brown gel.

General procedure to produce OH-RuMOP-based aerogels:

Once formed, the gel samples were washed with the same H_2O:DMF solvent mixture used for the synthesis. Next, they were soaked in acetone for three days, replacing the solvent every 12 h. Then, the resulting gels were dried by supercritical CO_2 at 14 MPa and 40 °C for 90 mins to yield the corresponding aerogel.

Table S1. Selected crystallographic data for **OH-RuMOP(OH)$_{12}$**

Empirical formula	$C_{224}H_{96}N_8O_{144}Ru_{24}$
Formula weight	7628.76
Temperature/K	200
Crystal system	tetragonal
Space group	*I*4/*m*
a/Å	30.9370(2)
b/Å	30.9370(2)
c/Å	31.2314(3)
α/°	90
β/°	90
γ/°	90
Volume/Å^3	29891.5(5)
Z	2
ρ_{calc}g/cm^3	0.848
μ/mm^{-1}	0.635
F(000)	7408.0
Crystal size/mm^3	0.2 × 0.2 × 0.2
Radiation	Mo Kα (λ = 0.71073)
2Θ range for data collection/°	3.706 to 52.742
Index ranges	-38 ≤ h ≤ 35, -34 ≤ k ≤ 35, -39 ≤ l ≤ 35
Reflections collected	123553
Independent reflections	15592 [R_{int} = 0.0367, R_{sigma} = 0.0232]
Data/restraints/parameters	15592/0/432
Goodness-of-fit on F^2	1.009
Final R indexes [I>=2σ (I)]	R_1 = 0.0505, wR_2 = 0.1402
Final R indexes [all data]	R_1 = 0.0624, wR_2 = 0.1533
Largest diff. peak/hole / e Å^{-3}	1.17/-1.04

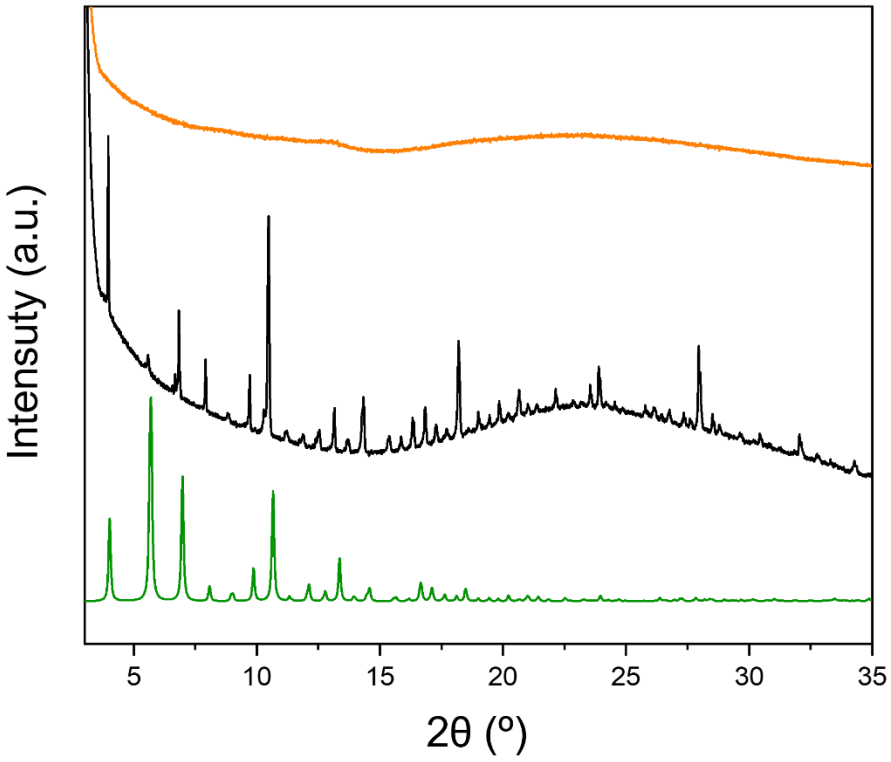

Figure S1. Powder X-ray diffraction patterns of as-made **OH-RuMOP(OH)$_{12}$** crystals (black) and bulk **OH-RuMOP[BF$_4$]$_{12}$** (orange) compared to simulated **OH-RuMOP(OH)$_{12}$** (green).

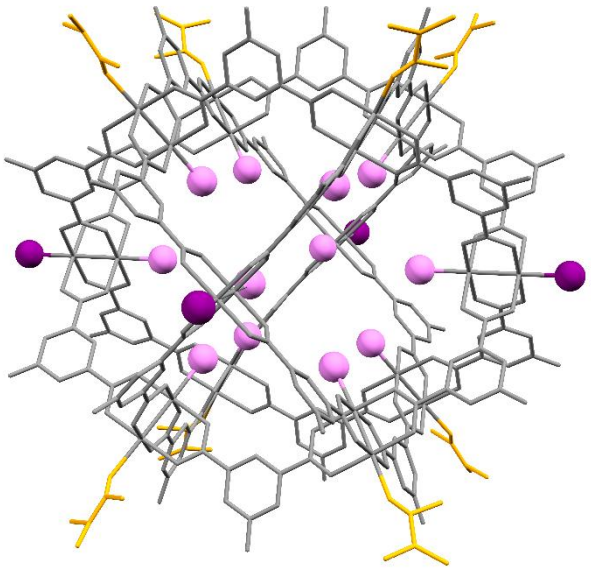

Figure S2. Representation of the structure of **OH-RuMOP(OH)$_{12}$** highlighting the occupancy of Ru_2 axial sites by eight external DMA molecules (orange), and indistinguishable four external (purple) and twelve internal (violet) H_2O/OH^- ligands.

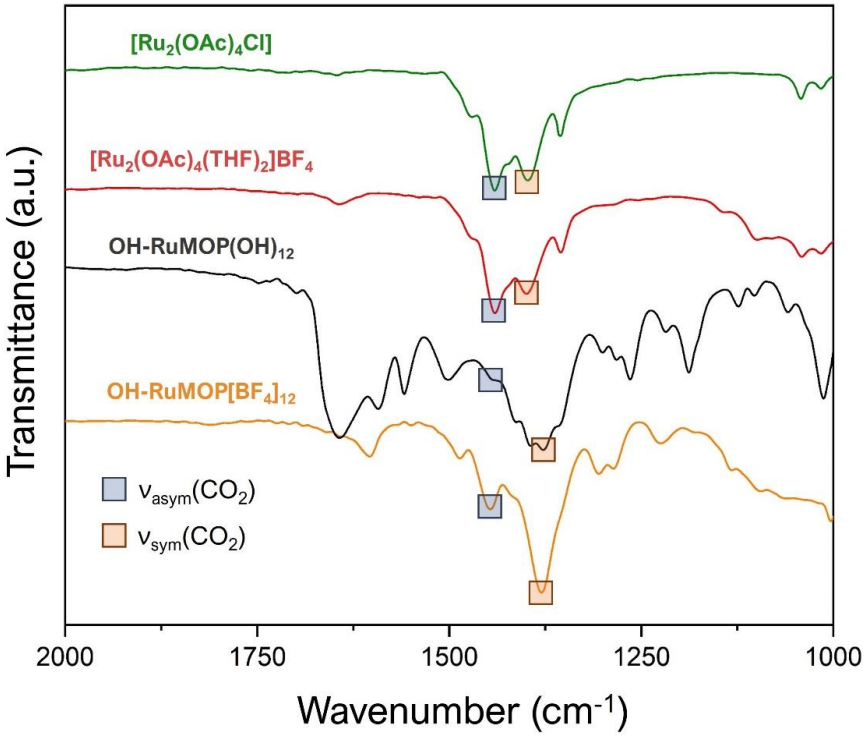

Figure S3. FT-IR spectra of $[Ru_2(OAc)_4Cl]$ (green), $[Ru_2(OAc)_4(THF)_2]BF_4$ (red), **OH-RuMOP(OH)$_{12}$** (black), and **OH-RuMOP[BF$_4$]$_{12}$** (orange), highlighting the symmetric, $\nu_{sym}(CO_2)$, and asymmetric, $\nu_{asym}(CO_2)$, carboxylate stretching modes.

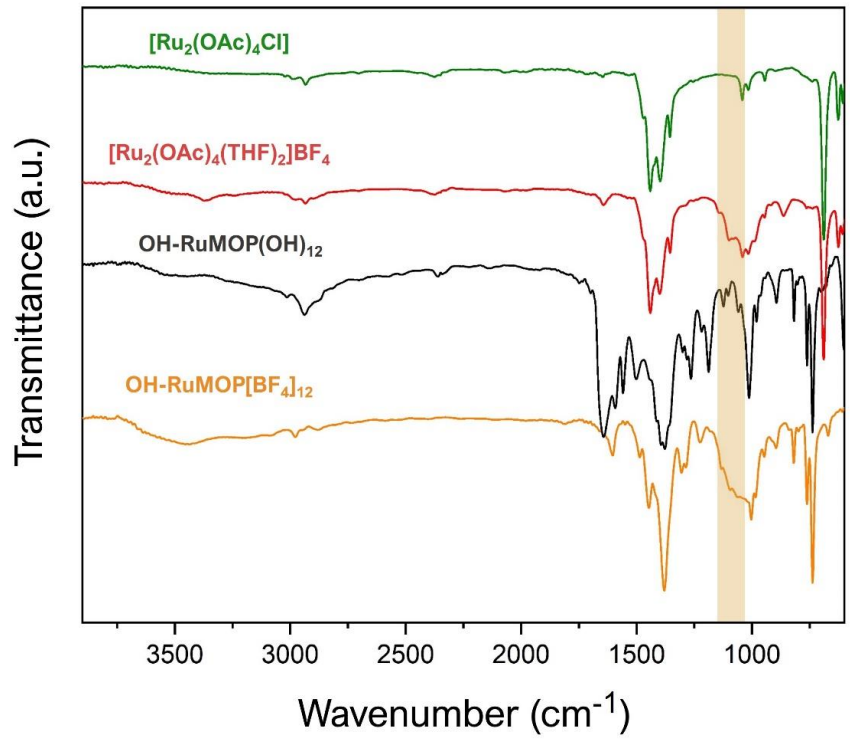

Figure S4. FT-IR spectra of $[Ru_2(OAc)_4Cl]$ (green), $[Ru_2(OAc)_4(THF)_2]BF_4$ (red), **OH-RuMOP(OH)$_{12}$** (black), and **OH-RuMOP[BF$_4$]$_{12}$** (orange), highlighting the presence/absence of BF_4^- at *ca.* 1050 cm^{-1}.

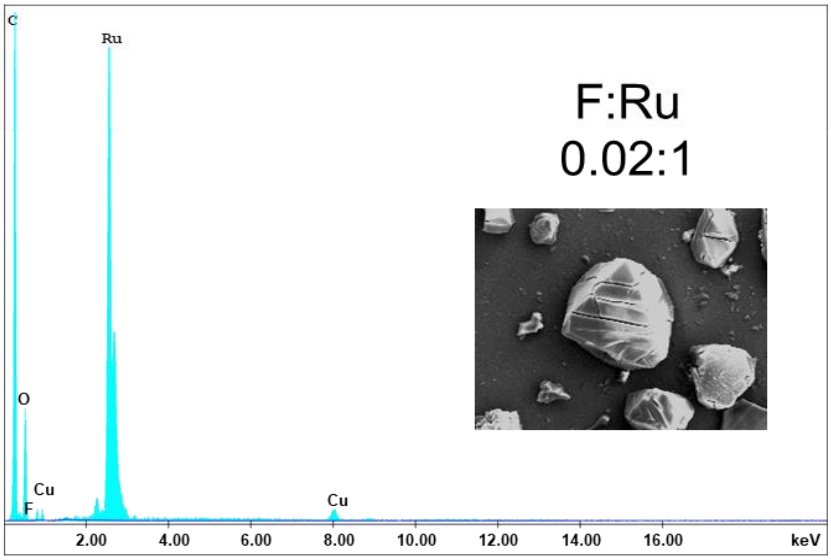

EDAX ZAF Quantification (Standardless)
Element Normalized
SEC Table : Default

Element	Wt %	At %	K-Ratio	Z	A	F
C K	32.80	60.55	0.2024	1.0982	0.5618	1.0001
O K	20.82	28.86	0.0269	1.0813	0.1195	1.0002
F K	0.13	0.15	0.0002	1.0169	0.1249	1.0004
RuL	43.93	9.64	0.4123	0.8388	1.1188	1.0000
CuK	2.32	0.81	0.0206	0.9077	0.9818	1.0000

Figure S5. EDX of **OH-RuMOP(OH)$_{12}$** crystals showing the F:Ru ratio.

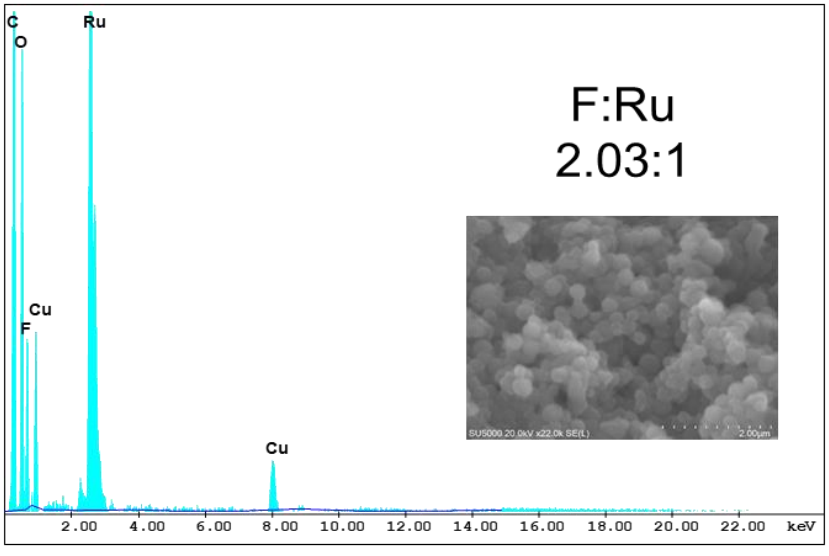

EDAX ZAF Quantification (Standardless)
Element Normalized
SEC Table : Default

Element	Wt %	At %	K-Ratio	Z	A	F
C K	32.40	51.42	0.1582	1.0706	0.4561	1.0003
O K	27.10	32.29	0.0431	1.0542	0.1509	1.0004
F K	10.06	10.09	0.0137	0.9915	0.1378	1.0004
RuL	26.41	4.98	0.2413	0.8124	1.1244	1.0000
CuK	4.04	1.21	0.0355	0.8799	0.9982	1.0000

Figure S6. EDX of **OH-RuMOP[BF$_4$]$_{12}$** powder showing the F:Ru ratio.

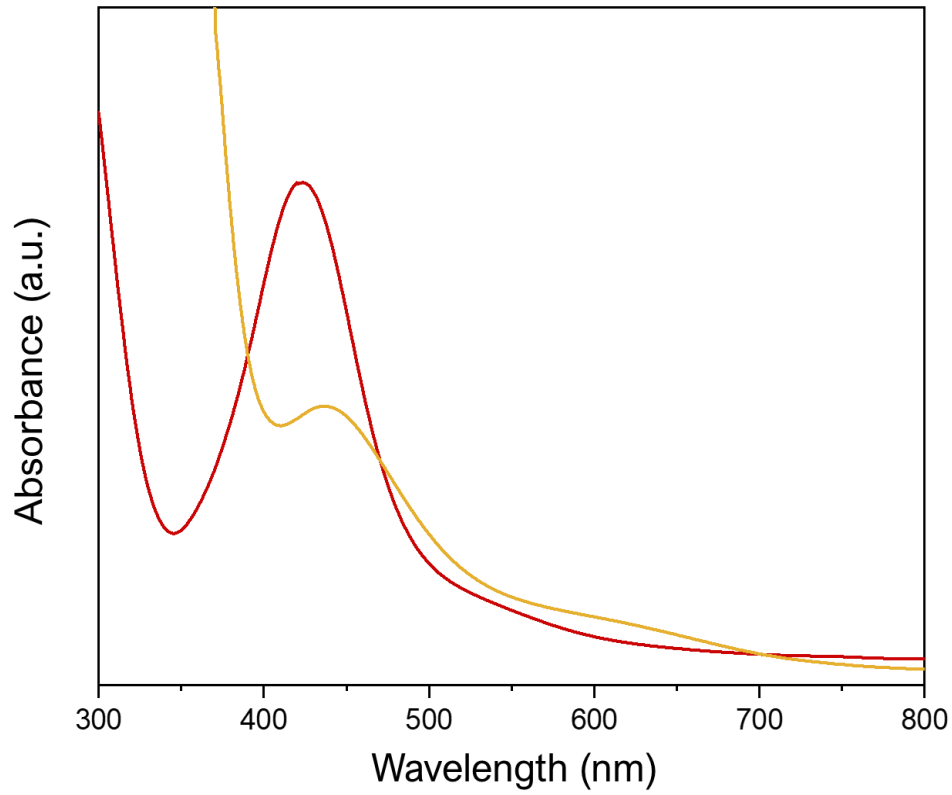

Figure S7. UV-vis spectra of $[Ru_2(OAc)_4]BF_4$ (red) and **OH-RuMOP[BF_4]$_{12}$** (orange) solutions in H_2O:DMF (9:1, v/v).

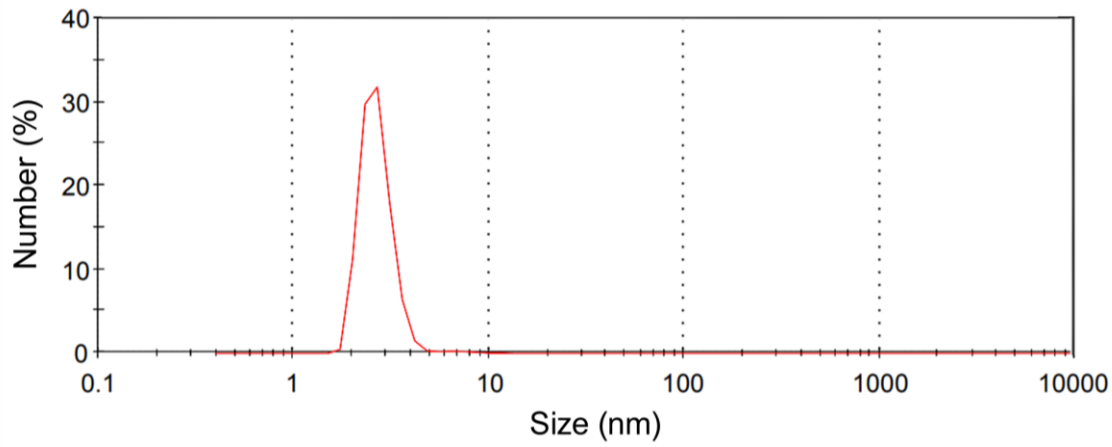

Figure S8. DLS measurement of **OH-RuMOP[BF_4]$_{12}$** in H_2O:DMF (9:1, v/v).

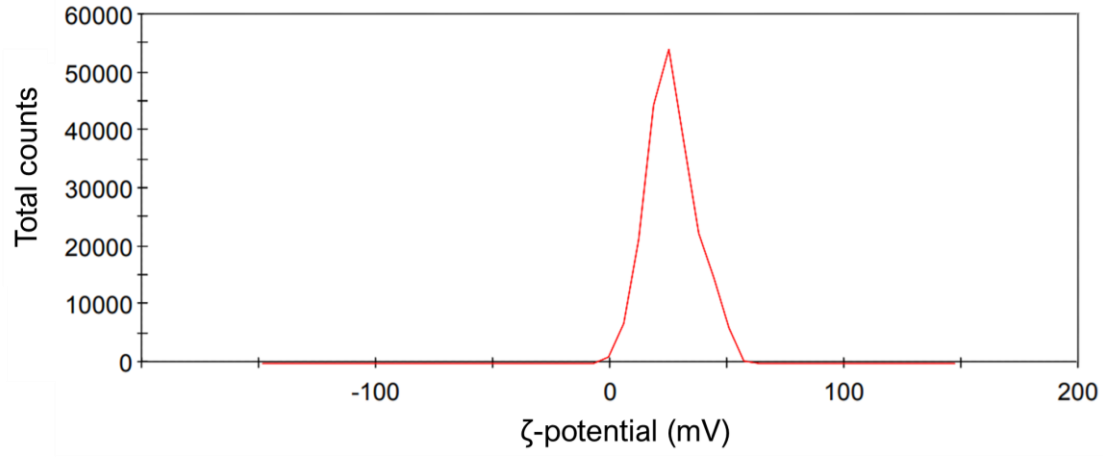

Figure S9. ζ-potential measurement of **OH-RuMOP[BF_4]$_{12}$** in H_2O:DMF (9:1, v/v).

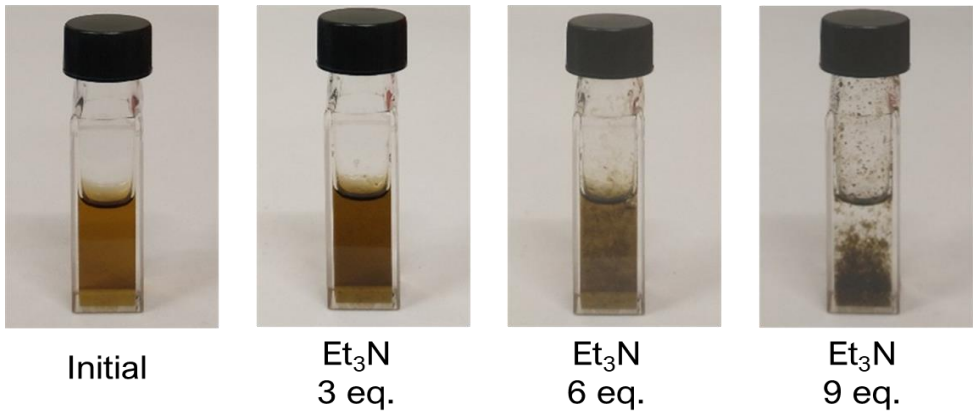

Figure S10. Photographs showing the evolution of a 0.2 mM **OH-RuMOP[BF_4]$_{12}$** H_2O:DMF (9:1, v/v) solution in the presence of increasing equivalents of triethylamine (Et_3N).

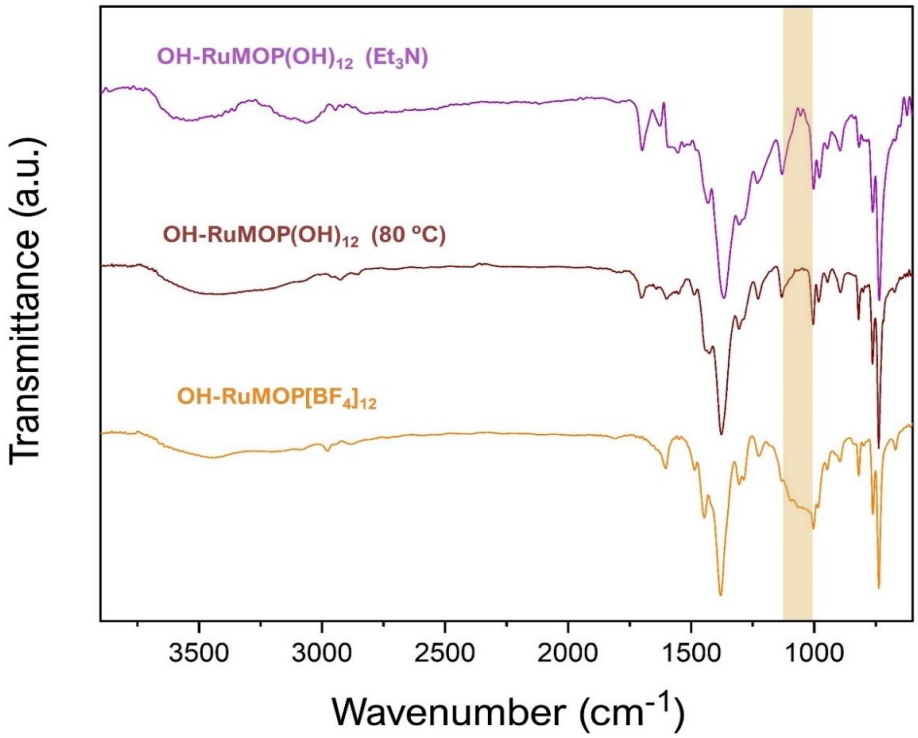

Figure S11. FT-IR spectra of **OH-RuMOP(OH)$_{12}$** solids obtained after treating a **OH-RuMOP[BF$_4$]$_{12}$** H_2O:DMF (9:1, v/v) solution with 9 equivalents of triethylamine (purple) or heating it at 80 °C for 24 h (brown), compared to **OH-RuMOP[BF$_4$]$_{12}$** powder, highlighting the presence/absence of BF_4^- at *ca.* 1050 cm^{-1}.

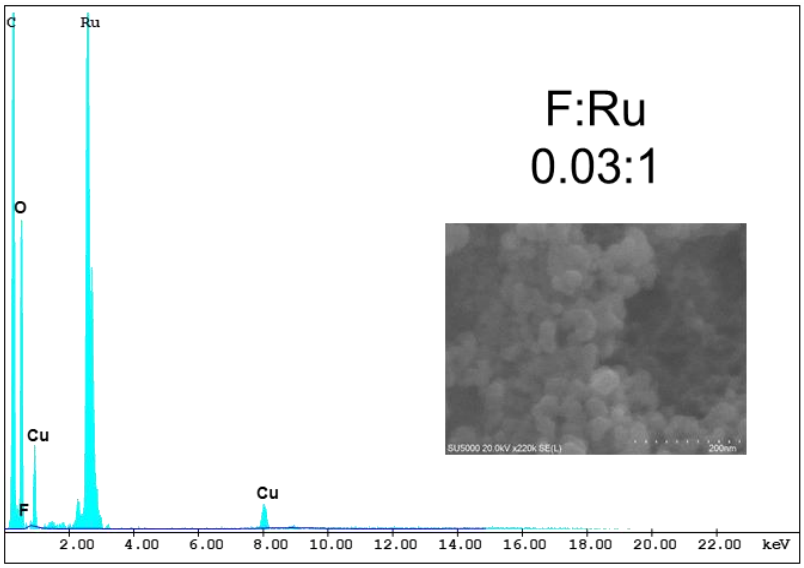

EDAX ZAF Quantification (Standardless)
Element Normalized
SEC Table : Default

Element	Wt %	At %	K-Ratio	Z	A	F
C K	30.50	53.48	0.1998	1.0939	0.5986	1.0002
O K	28.74	37.84	0.0452	1.0754	0.1461	1.0001
F K	0.21	0.24	0.0003	1.0106	0.1426	1.0003
RuL	40.55	8.45	0.3657	0.8203	1.0996	1.0000

Figure S12. EDX of **OH-RuMOP(OH)$_{12}$**, obtained after addition of 9 equivalents of triethylamine (Et_3N) to a **OH-RuMOP[BF$_4$]$_{12}$** H_2O:DMF (9:1, v/v) solution, showing the F:Ru ratio.

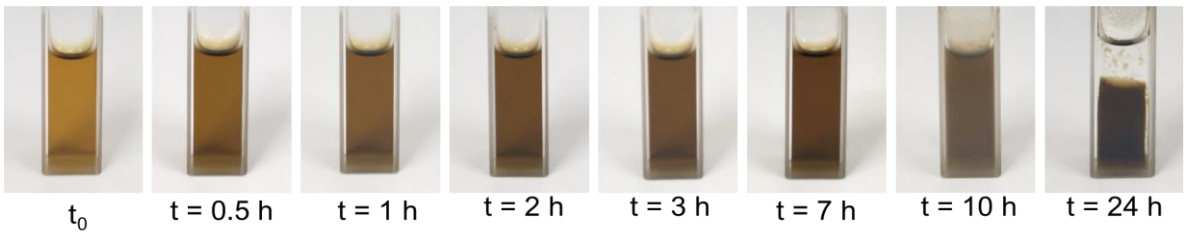

Figure S13. Photographs showing the evolution of a 0.2 mM **OH-RuMOP[BF$_4$]$_{12}$** H_2O:DMF (9:1, v/v) solution upon heating at 80 °C for 24 h.

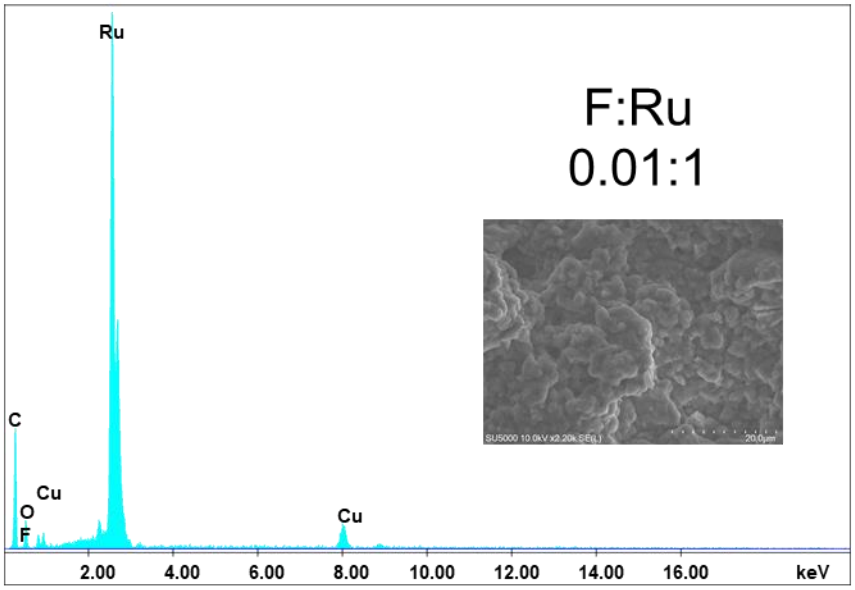

EDAX ZAF Quantification (Standardless)
Element Normalized
SEC Table : Default

Element	Wt %	At %	K-Ratio	Z	A	F
C K	11.89	42.39	0.0683	1.1929	0.4819	1.0001
O K	8.11	21.71	0.0095	1.1742	0.0995	1.0003
F K	0.13	0.30	0.0002	1.1041	0.1184	1.0007
RuL	72.93	30.92	0.6876	0.9246	1.0196	1.0000
CuK	6.94	4.68	0.0660	0.9981	0.9523	1.0000

Figure S14. EDX of **OH-RuMOP(OH)$_{12}$**, obtained after heating a **OH-RuMOP[BF$_4$]$_{12}$** H_2O:DMF (9:1, v/v) solution at 80 °C for 24 h, showing the F:Ru ratio.

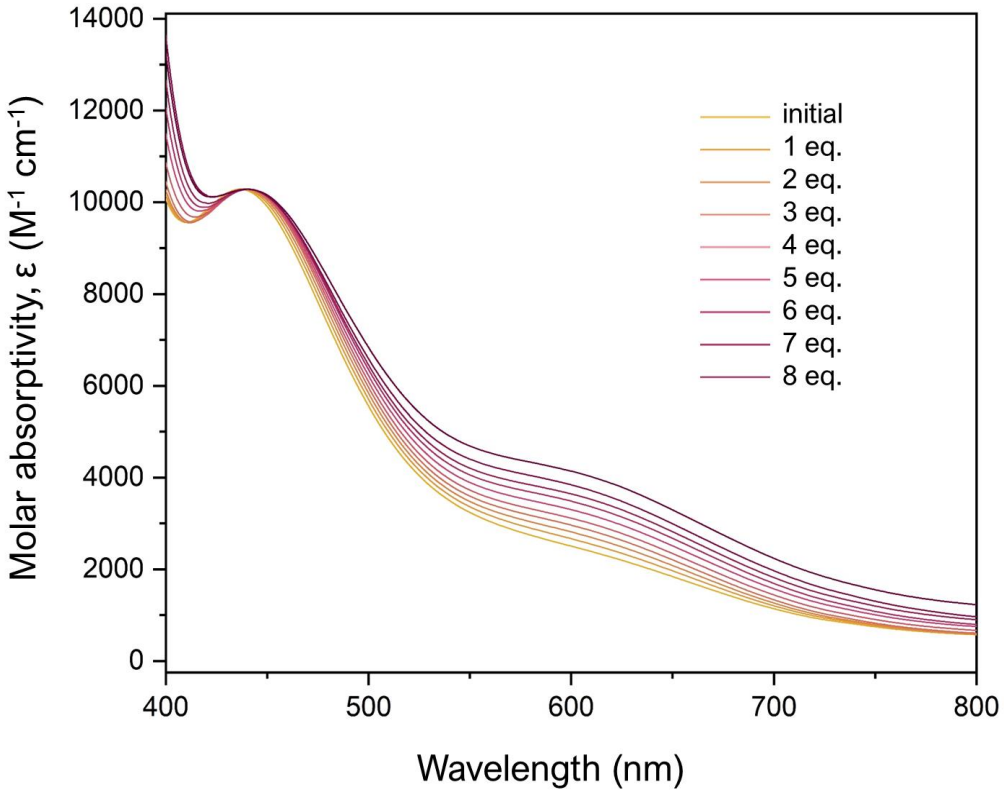

Figure S15. UV-vis spectra (top) and photographs (bottom) showing the evolution of a 0.2 mM **OH-RuMOP[BF_4]$_{12}$** H_2O:DMF (9:1, v/v) solution in the presence of increasing equivalents of triethylamine (Et_3N).

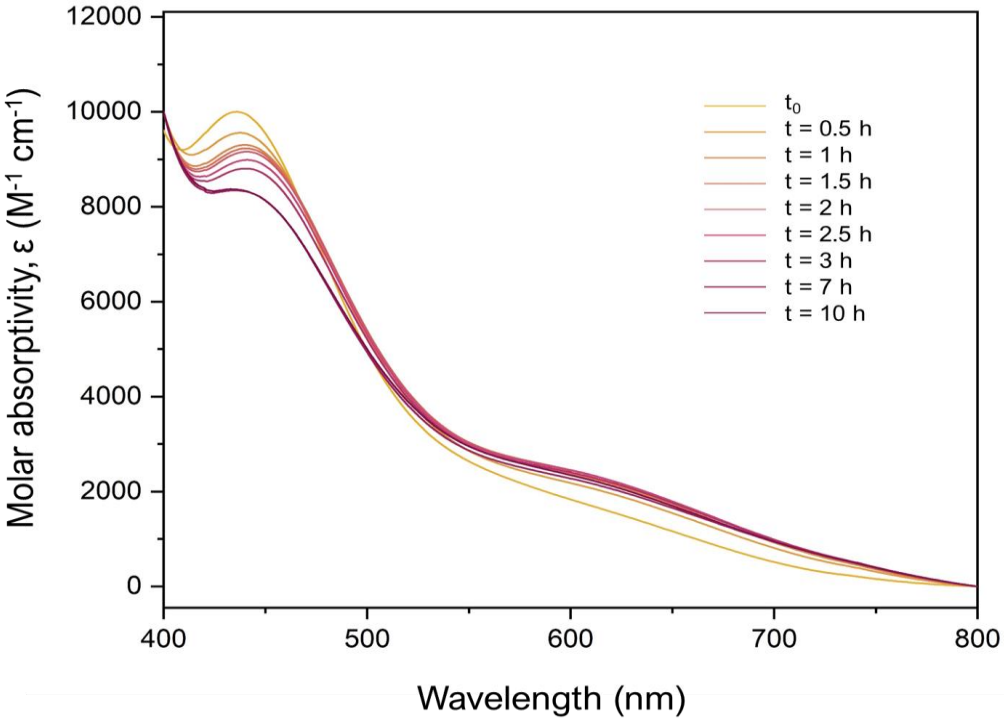

Figure S16. UV-vis spectra (top) and photographs (bottom) showing the evolution of a 0.2 mM **OH-RuMOP[BF_4]$_{12}$** H_2O:DMF (9:1, v/v) solution upon heating at 80 °C for 10 h.

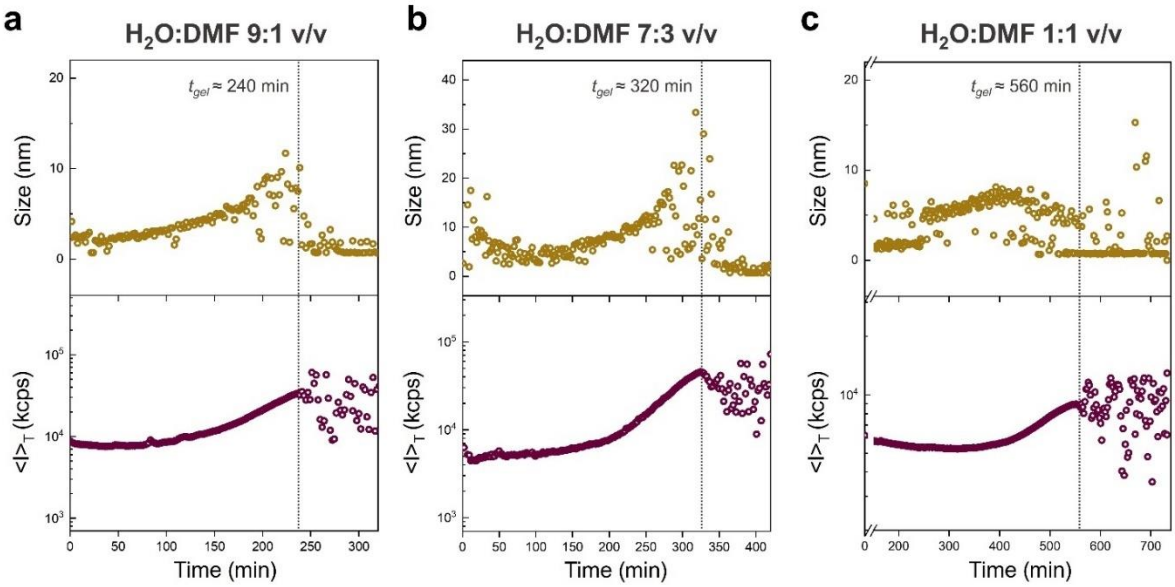

Figure S17. Time-resolved dynamic light scattering experiments (TR-DLS) during the thermo-induced self-gelation at 70 °C of **OH-RuMOP[BF_4]$_{12}$** solutions (1 mM) in H_2O:DMF 9:1 v/v (a), 7:3 v/v (b), and 1:1 v/v (c) solvent mixtures.

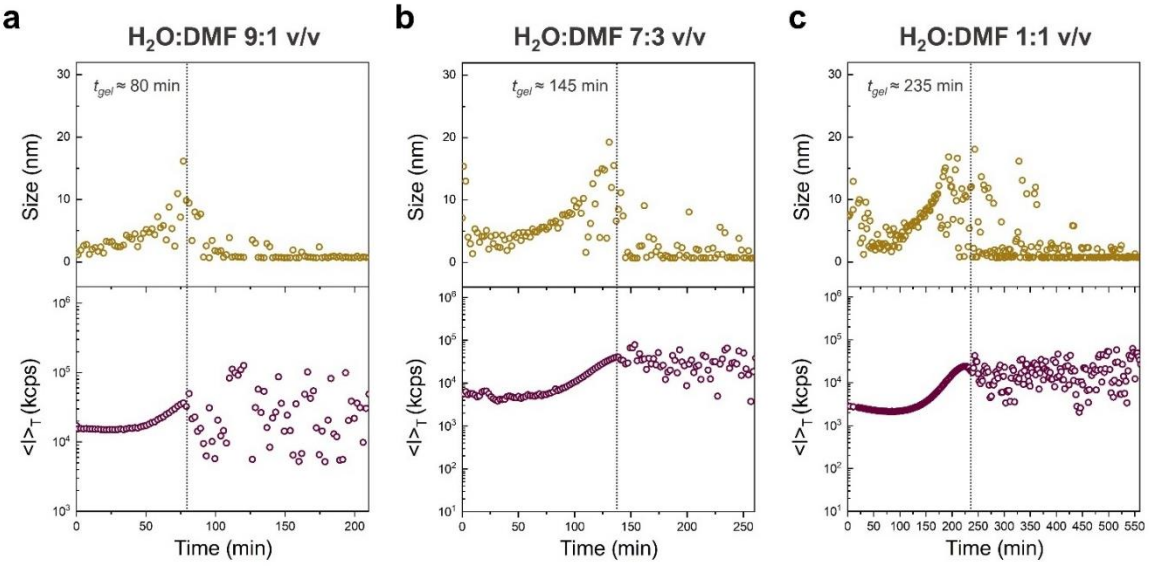

Figure S18. Time-resolved dynamic light scattering experiments (TR-DLS) during the thermo-induced self-gelation at 80 °C of **OH-RuMOP[BF_4]$_{12}$** solutions (1 mM) in H_2O:DMF 9:1 v/v (a), 7:3 v/v (b), and 1:1 v/v (c) solvent mixtures.

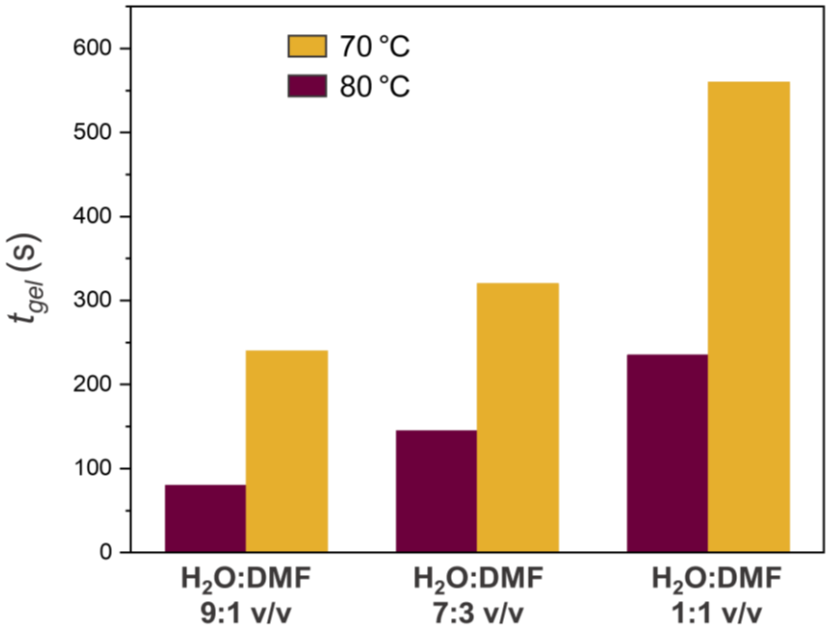

Figure S19. Estimated gelation time (t_{gel}) values for thermo-induced self-gelation of **OH-RuMOP[BF_4]$_{12}$** solutions (1 mM) in H_2O:DMF 9:1 v/v, 7:3 v/v, and 1:1 v/v at 70 °C and 80 °C.

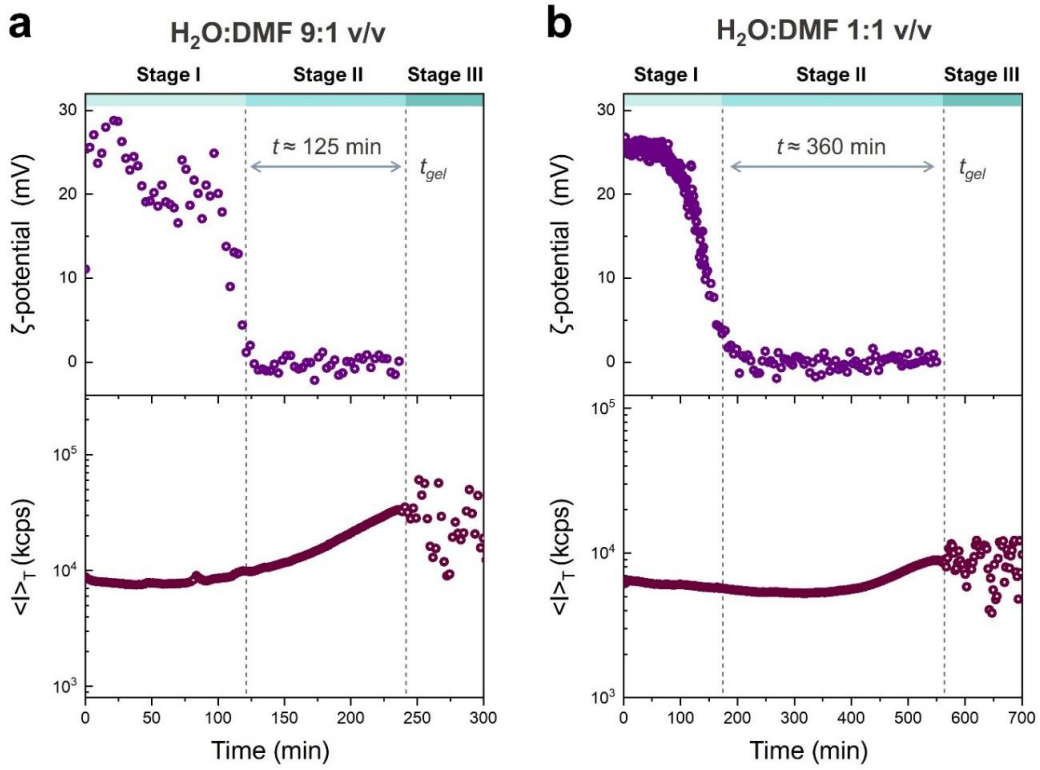

Figure S20. Comparison between ζ-potential and $\langle I \rangle_T$ data of 1 mM **OH-RuMOP[BF_4]$_{12}$** solutions in H_2O:DMF 9:1 v/v (a), and 1:1 v/v (b) during the thermo-induced self-gelation at 70 °C

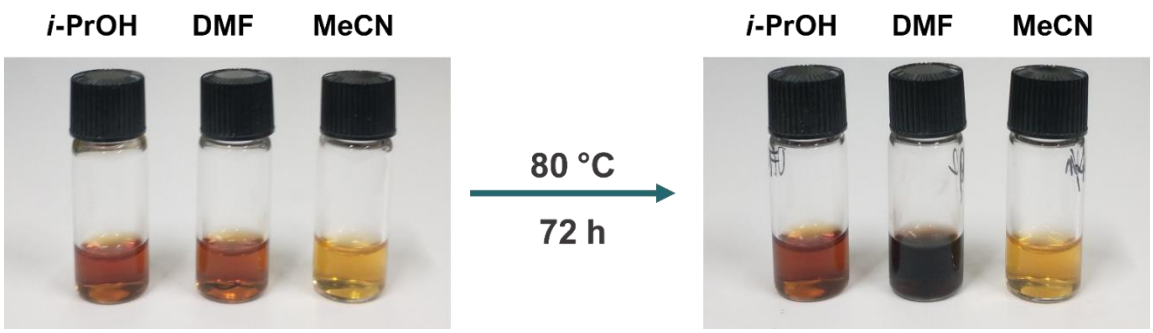

Figure S21. Photographs of **OH-RuMOP[BF_4]$_{12}$** solutions in *i*-PrOH (1 mM), DMF (1 mM), and MeCN (0.5 mM), before (left) and after (right) heating at 80 °C for 72 h.

Figure S22. Thixotropic behavior of the gel obtained after 3 h heating at 80 °C, showing reversible sol-gel transition upon shaking/resting.

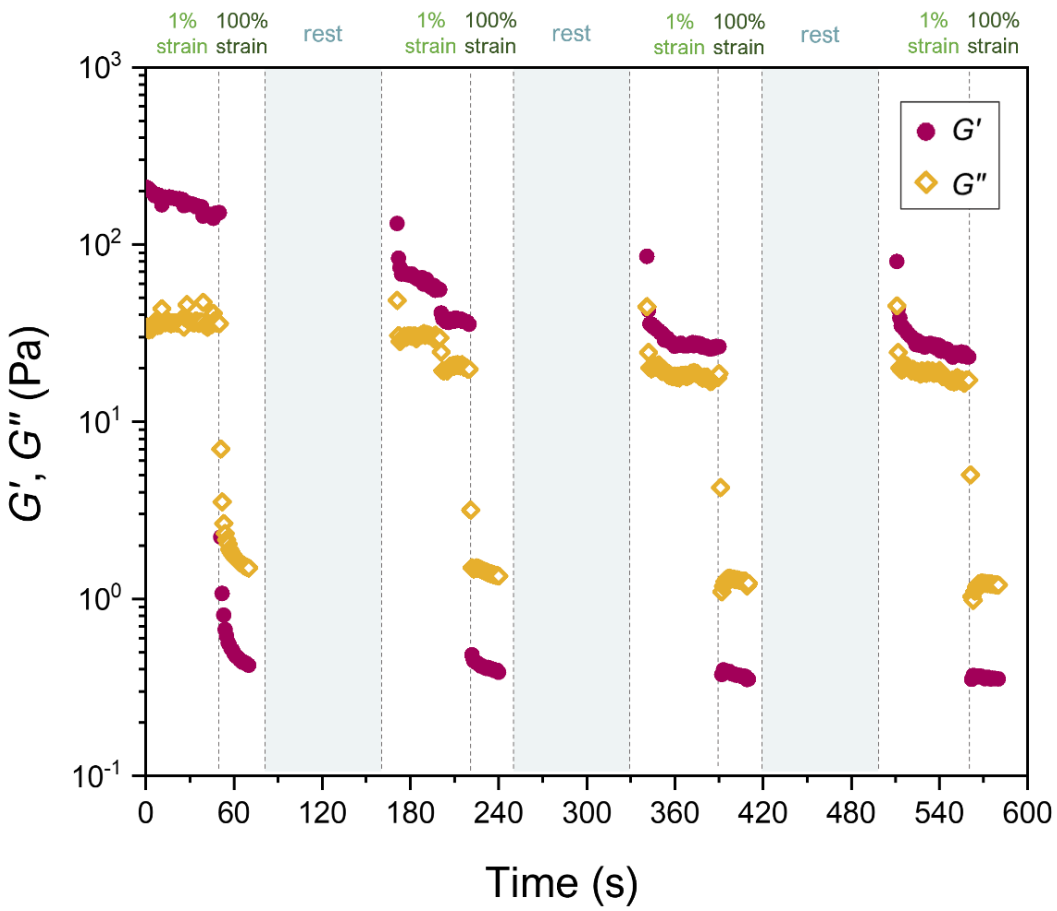

Figure S23. Step strain experiments of the gel obtained after 3 h heating at 80 °C. Under 1% strain *G′* (storage modulus) remains higher than *G″* (loss modulus), which corresponds to a gel phase. Under 100% strain gel is converted to the sol phase where *G″* is higher than *G′*. After 100 s resting, sol is reverted to the gel phase as *G′* is greater than *G″*. This is repeated for two more cycles to show self-recovering properties of the gel.

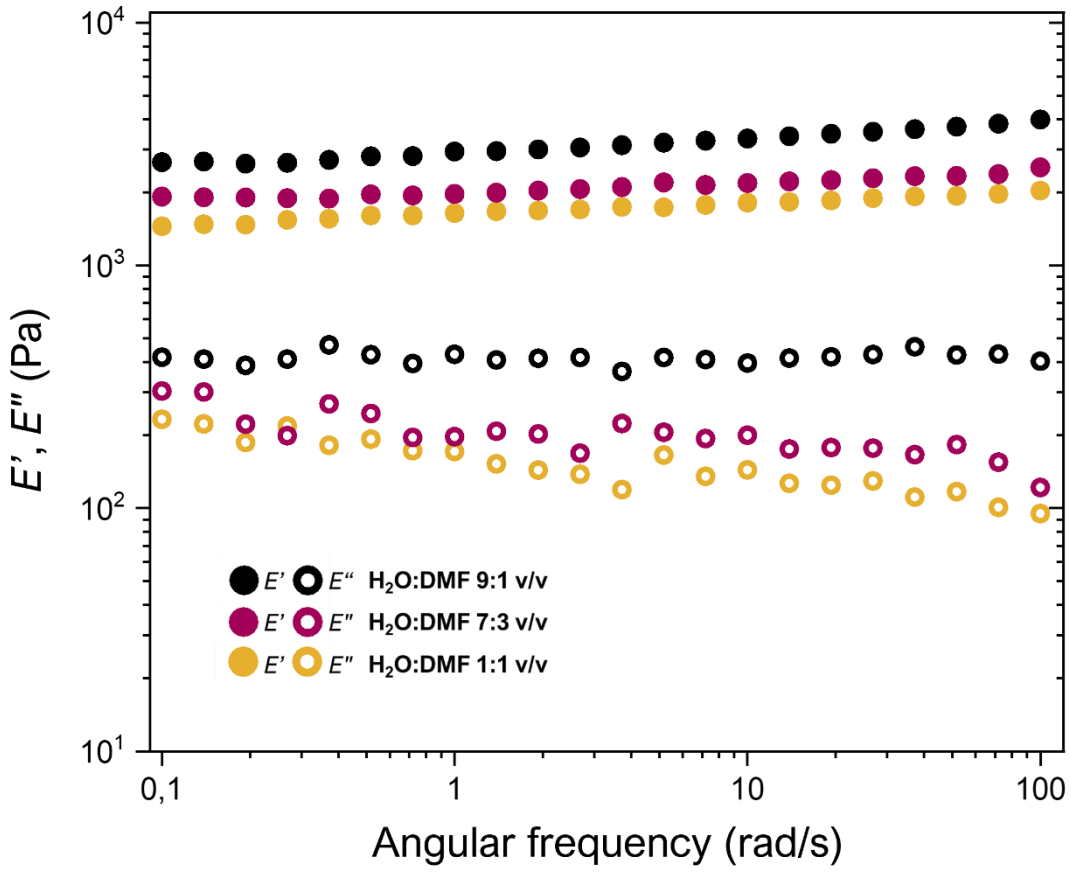

Figure S24. Storage and loss Young's modulus, *E'* and *E''* respectively, of the gels formed by thermo-induced self-gelation of **OH-RuMOP[BF_4]$_{12}$** solutions (1 mM) in H_2O:DMF 9:1 v/v (black), 7:3 v/v (magenta), and 1:1 v/v (yellow) heated at 80 °C for 24 h. The measurements were performed at a fixed strain amplitude (1%)

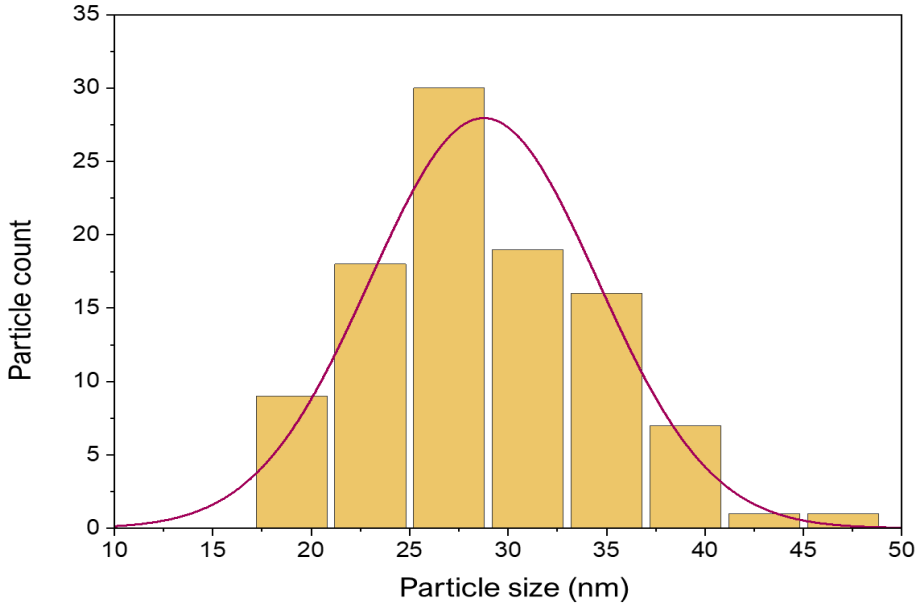

Figure S25. Particle size distribution histogram of **OH-RuMOP-agel** determined from FE-SEM images.

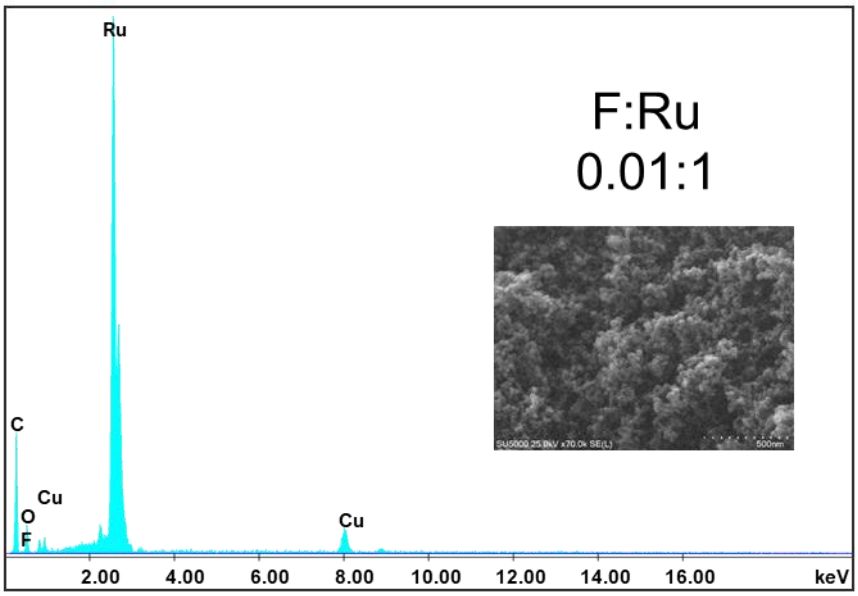

EDAX ZAF Quantification (Standardless)
Element Normalized
SEC Table : Default

Element	Wt %	At %	K-Ratio	Z	A	F
C K	11.89	42.39	0.0683	1.1929	0.4819	1.0001
O K	8.11	21.71	0.0095	1.1742	0.0995	1.0003
F K	0.13	0.30	0.0002	1.1041	0.1184	1.0007
RuL	72.93	30.92	0.6876	0.9246	1.0196	1.0000

Figure S26. EDX of **OH-RuMOP-agel** showing the F:Ru ratio.

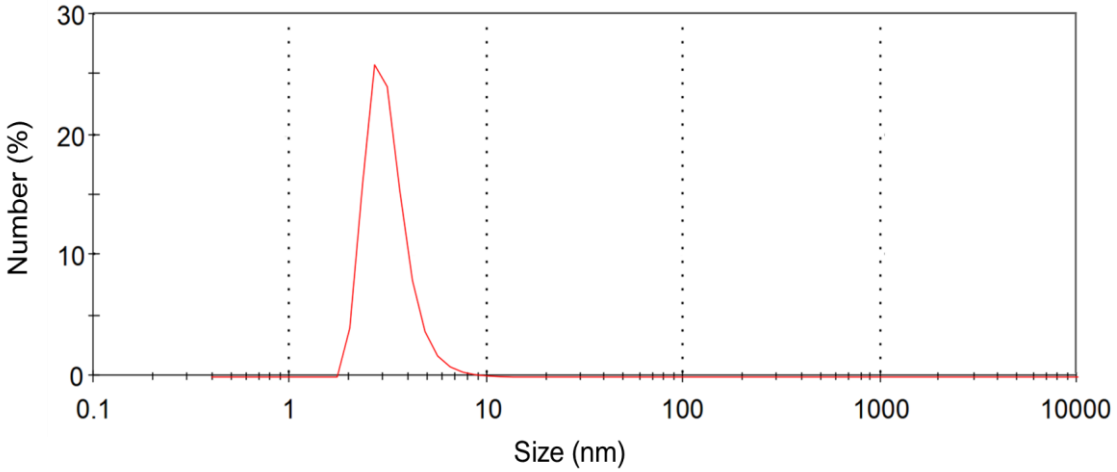

Figure S27. DLS measurement of the solution obtained after dissolving **OH-RuMOP-agel** in HBF_4/DMF.

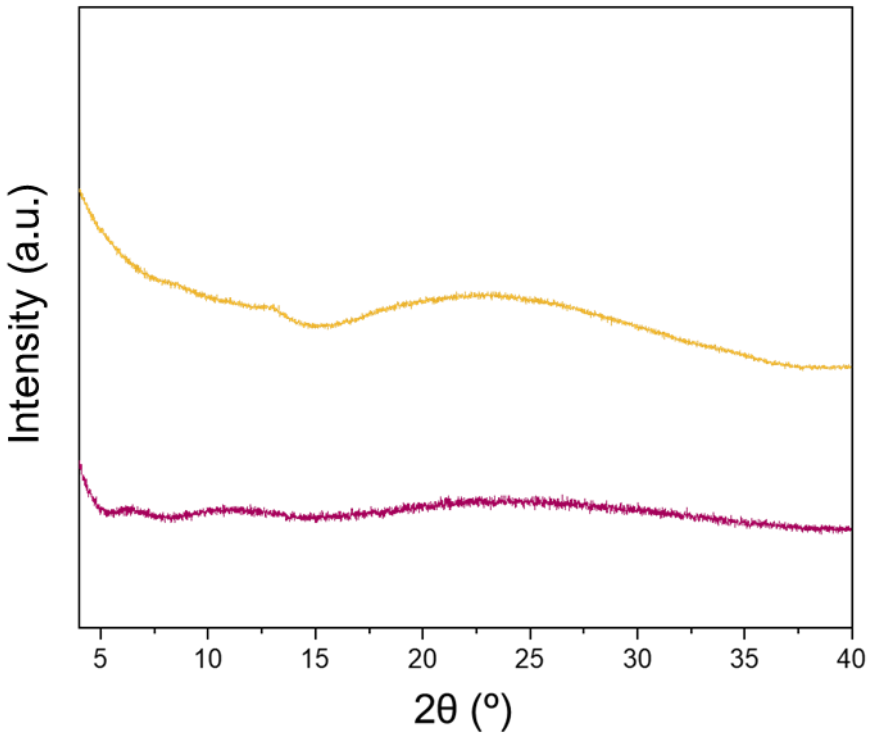

Figure S28. Powder X-ray diffraction patterns of **OH-RuMOP-agel** (magenta) and bulk **OH-RuMOP[BF_4]$_{12}$** (orange).

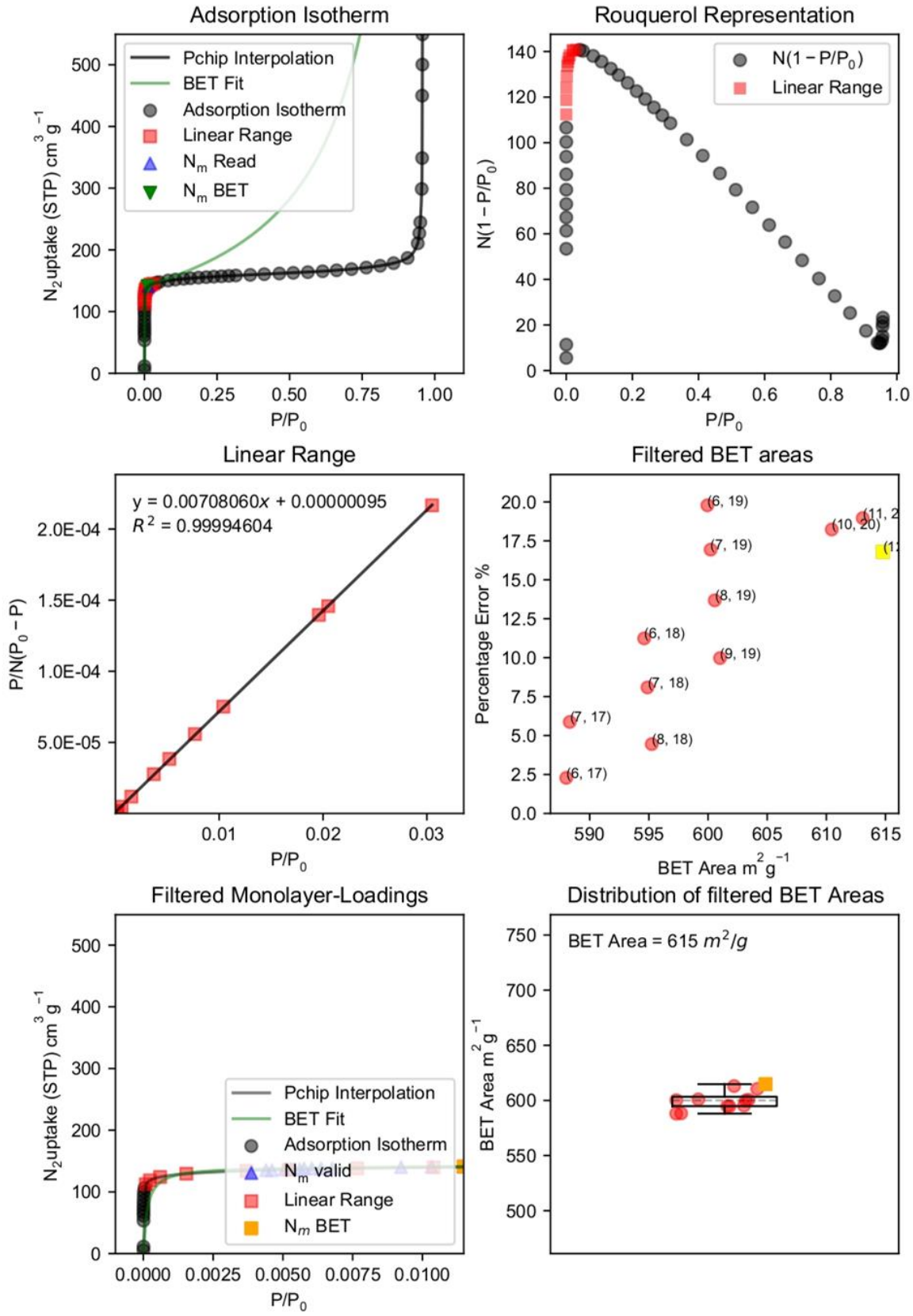

Figure S29. BETSI analysis of **OH-RuMOP[BF_4]$_{12}$.**

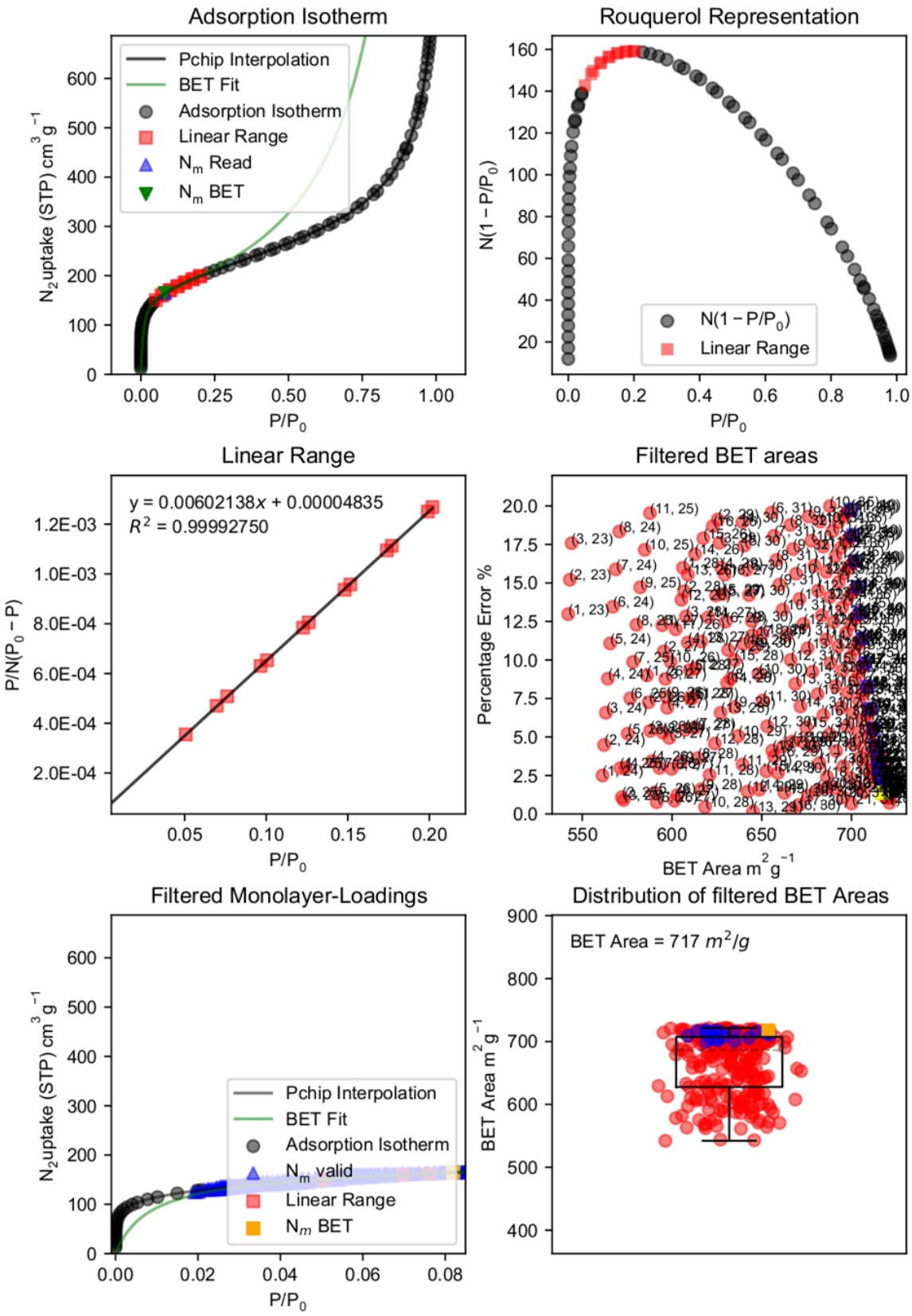

Figure S30. BETSI analysis of **OH-RuMOP-agel.**

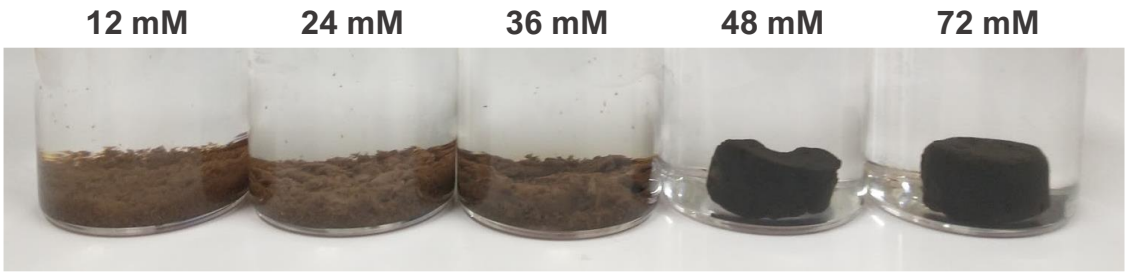

Figure S31. Photographs of the resulting products after heating H_2O-DMF 9:1 v/v mixtures containing $[Ru_2(OAc)_4(THF)_2]BF_4$ and 5-hydroxyisophthalic acid (1:4) at different concentrations ($[Ru_2]$ = 12 to 72 mM) were heated at 80 °C for 24 h.

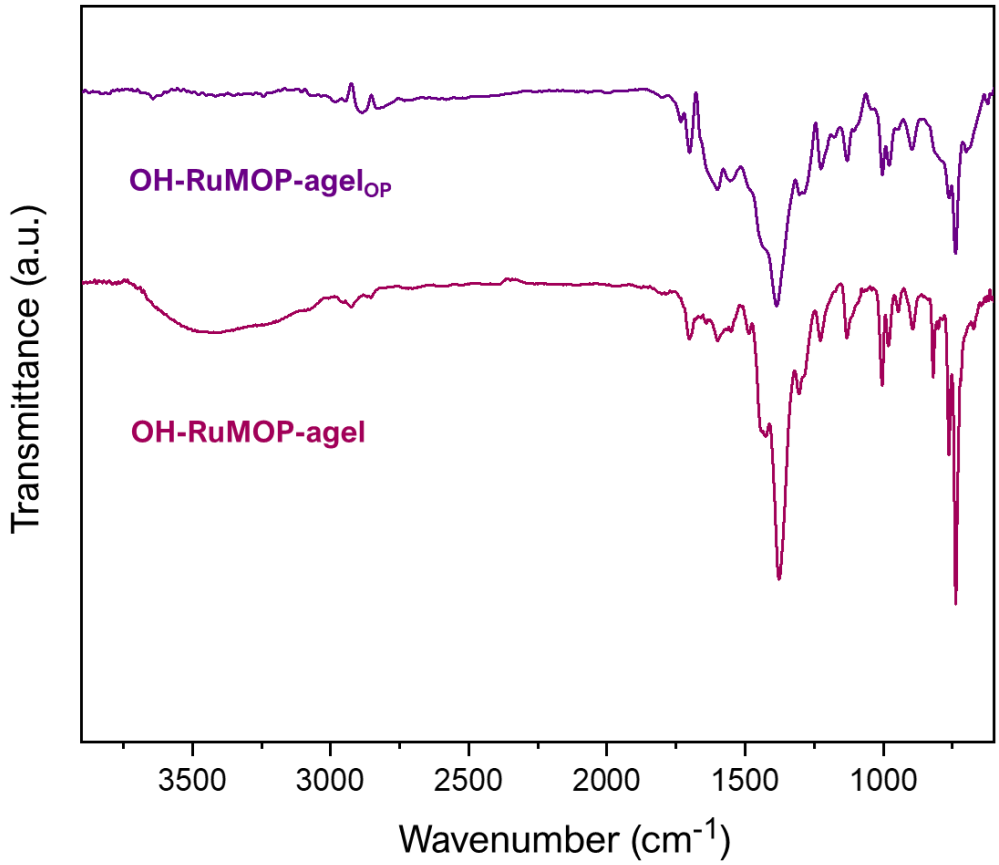

Figure S32. FT-IR spectra of **OH-RuMOP-agel** (magenta) and **OH-RuMOP-agel$_{OP}$** (purple).

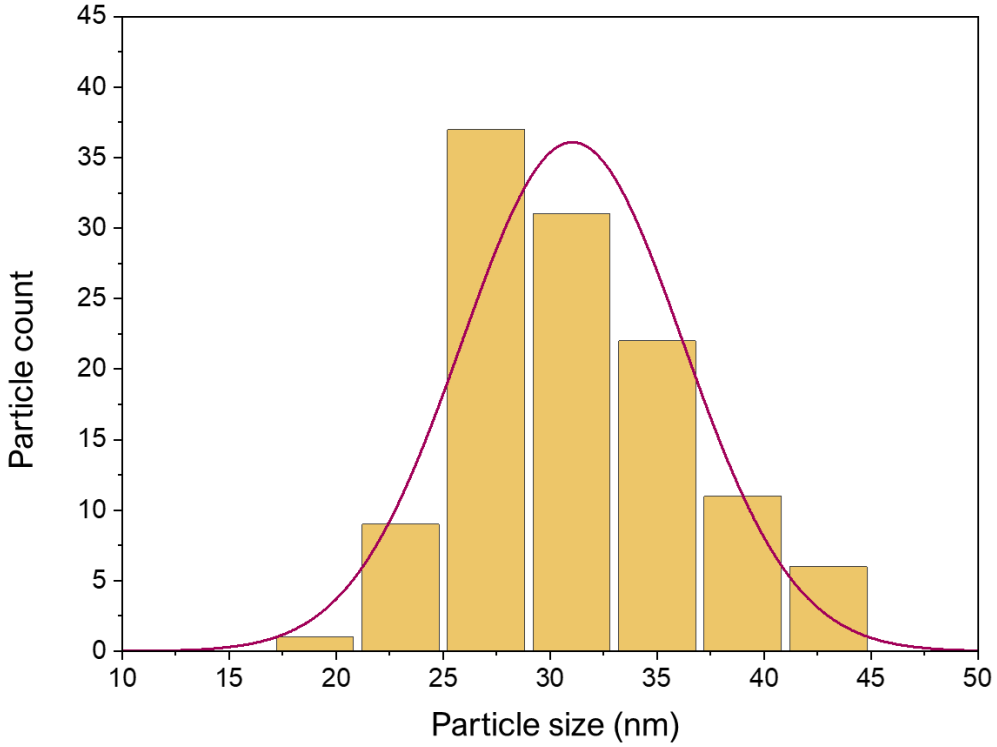

Figure S33. Particle size distribution histogram of **OH-RuMOP-agel$_{OP}$** determined from FE-SEM images.

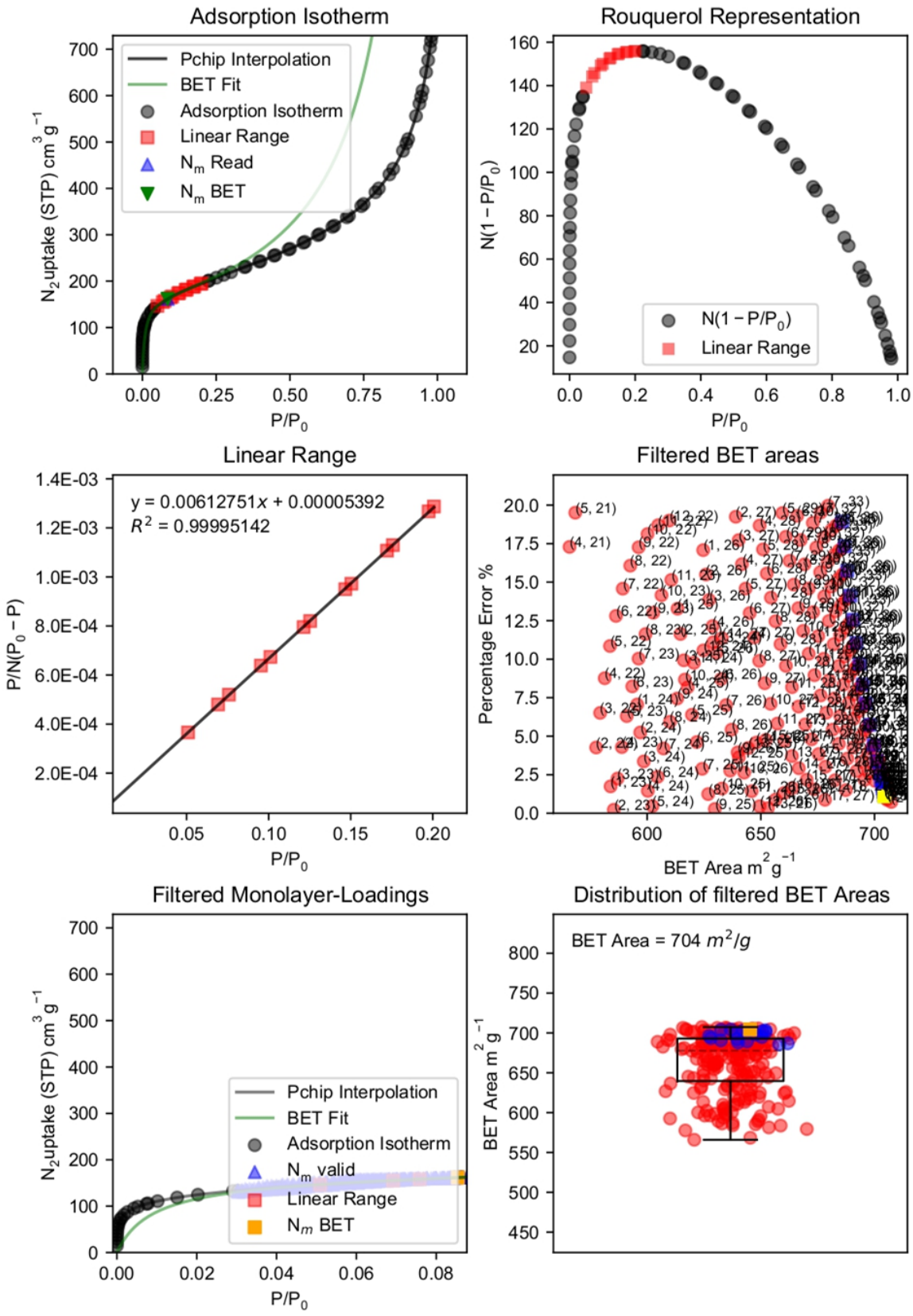

Figure S34. BETSI analysis of **OH-RuMOP-agel$_{OP}$.**

References:

1. Sheldrick, G. M. Crystal structure refinement with SHELXL. *Acta Cryst.*, 2015, C71, 3–8.

2. Dolomanov, O. V., Bourhis, L. J., Gildea, R. J., Howard, J. A. K. & Puschmann, H. (2009). OLEX2: a complete structure solution, refinement and analysis program. *J. Appl. Cryst*. 2009, **42**, 339–341.

3. Osterrieth, J. W. M., Rampersad, J., Madden, D., Rampal, N., Skoric, L., Connolly, B., Allendorf, M. D., Stavila, V., Snider, J. L., Ameloot, R., Marreiros, J., Ania, C., Azevedo, D., Vilarrasa-Garcia, E., Santos, B. F., Bu, X.-H., Chang, Z., Bunzen, H., Champness, N. R., Griffin, S. L., Chen, B., Lin, R.-B., Coasne, B., Cohen, S., Moreton, J. C., Colón, Y. J., Chen, L., Clowes, R., Coudert, F.-X., Cui, Y., Hou, B., D'Alessandro, D. M., Doheny, P. W., Dincă, M., Sun, C., Doonan, C., Huxley, M. T., Evans, J. D., Falcaro, P., Ricco, R., Farha, O., Idrees, K. B., Islamoglu, T., Feng, P., Yang, H., Forgan, R. S., Bara, D., Furukawa, S., Sanchez, E., Gascon, J., Telalović, S., Ghosh, S. K., Mukherjee, S., Hill, M. R., Sadiq, M. M., Horcajada, P., Salcedo-Abraira, P., Kaneko, K., Kukobat, R., Kenvin, J., Keskin, S., Kitagawa, S., Otake, K.-i., Lively, R. P., DeWitt, S. J. A., Llewellyn, P., Lotsch, B. V., Emmerling, S. T., Pütz, A. M., Martí-Gastaldo, C., Padial, N. M., García-Martínez, J., Linares, N., Maspoch, D., Suárez del, J. A., Moghadam, P., Oktavian, R., Morris, R. E., Wheatley, P. S., Navarro, J., Petit, C., Danaci, D., Rosseinsky, M. J., Katsoulidis, A. P., Schröder, M., Han, X., Yang, S., Serre, C., Mouchaham, G., Sholl, D. S., Thyagarajan, R., Siderius, D., Snurr, R. Q., Goncalves, R. B., Telfer, S., Lee, S. J., Ting, V. P., Rowlandson, J. L., Uemura, T., Iiyuka, T., van der, M. A., Rega, D., Van, V., Rogge, S. M. J., Lamaire, A., Walton, K. S., Bingel, L. W., Wuttke, S., Andreo, J., Yaghi, O., Zhang, B., Yavuz, C. T., Nguyen, T. S., Zamora, F., Montoro, C., Zhou, H., Kirchon, A., Fairen-Jimenez, D., How Reproducible are Surface Areas Calculated from the BET Equation?. *Adv. Mater.* 2022, **34**, 2201502

4. Urbanos F.A., Barral M.C., Jiménez-Aparicio R., Synthesis and properties of some diruthenium acetate compounds. *Polyhedron* 1998, **7**, 24, 2597-2600.